Detecting dynamical interdependence and generalized synchrony through mutual prediction in a neural ensemble

Steven J. Schiff, Paul So, and Taeun Chang
Center for Neuroscience, Children's Research Institute, and Department of Neurosurgery, Children's National Medical Center and The George Washington University, 111 Michigan Avenue, NW, Washington, D.C. 20010

Robert E. Burke
Laboratory of Neural Control, National Institutes of Health, National Institute of Neurological Diseases and Stroke, Bethesda, Maryland 20892

Tim Sauer
Department of Mathematics, George Mason University, Fairfax, Virginia 22030
(Recieved 14 May 1996; revised manuscript received 2 August 1996)

A method to characterize dynamical interdependence among nonlinear systems is derived based on mutual nonlinear prediction. Systems with nonlinear correlation will show mutual nonlinear prediction when standard analysis with linear cross correlation might fail. Mutual nonlinear prediction also provides information on the directionality of the coupling between systems. Furthermore, the existence of bidirectional mutual nonlinear prediction in unidirectionally coupled systems implies generalized synchrony. Numerical examples studied include three classes of unidirectionally coupled systems: systems with identical parameters, nonidentical parameters, and stochastic driving of a nonlinear system. This technique is then applied to the activity of motoneurons within a spinal cord motoneuron pool. The interrelationships examined include single neuron unit firing, the total number of neurons discharging at one time as measured by the integrated monosynaptic reflex, and intracellular measurements of integrated excitatory postsynaptic potentials (EPSP's). Dynamical interdependence, perhaps generalized synchrony, was identified in this neuronal network between simultaneous single unit firings, between units and the population, and between units and intracellular EPSP's. [S1063-651X(96)04012-3]

PACS number(s): 87.10.+e, 05.45.+b

I. INTRODUCTION

When the dynamical behaviors of two systems are observed, how can we tell if they are coupled? Traditionally, one tests to see if there is a degree of correlation between variables observed from each system. In systems with many components, cross correlation in the time domain and cross spectrum or coherence in the frequency domain have long been the mainstays of correlation detection [1]. Cross correlation measures the linear correlation between two variables, and the cross spectrum is the Fourier transform of the cross correlation. Measures of cross correlation or coherency in effect ask whether there exists a functional relationship between the time series in question. The functional relation is albeit a very specific one for these linear measures. Nevertheless, for linear systems, these linear measurements are sufficient to describe the dynamical interdependence of their parts. Unfortunately, the components of complex extended systems in nature rarely display only a linear interdependence, and superposition may break down in describing their aggregate behavior.

A broader definition of dynamical interdependence was recently offered by Pecora, Caroll, and Heagy [2], who suggested that dynamical interdependence implies that observed variables come from the same dynamical system. We wish to take two arbitrary nonlinear systems, whose underlying dynamical equations are unknown to us, and ask whether their variables are interdependent. Finding evidence of dynamical interdependence in such systems implies two things: either the systems communicate (they are coupled together and information flows between them), or they are coupled to a common driver.

In the case when two arbitrary nonlinear systems are coupled, it is possible that their temporal evolutions might become ''synchronized'' as one adjusts the coupling strength between them, even though their temporal evolutions will not be identical. One of the earliest discussions of this topic was Afraimovich, Verichev, and Ravinovich [3], who described a state they termed ''stochastic synchronization'' that occurred between nonidentical nonlinear oscillators with dissipative coupling. Stochastic synchrony was here defined as the existence of a topological identity (homeomorphic or diffeomorphic) between the attractors describing each nonlinear oscillator of the system. Note here that knowledge of the separable state variables for each subsystem was assumed. The term *generalized synchrony* was later applied by Rulkov *et al.* [4] to unidirectionally coupled systems with such ''synchronized'' behaviors. In [4], through the restriction of unidirectional coupling, delay coordinate embedding variables [5] could be used to establish a topological identity. Rulkov *et al.* [4] further defined a mutual false nearest neighbor statistic to establish continuity, and thus infered the existence of generalized synchrony in such systems. Pecora, Carroll, and Heagy [6] explored the statistics that define the nature of the topological relationship between two time series from such coupled systems, in an effort to define

whether the function that links the systems is continuous or differentiable. Generalized synchrony is therefore a particular case of dynamical interdependence [2].

When two systems are coupled to a common driver, if the coupling is sufficiently strong to establish generalized synchrony between the driver and the response systems (assumed to be identical), then the two response systems will become asymptotically stable and thus synchronize [7]. Under such conditions, the two response systems will synchronize after a finite transient irrespective of their initial conditions. When this occurs, the largest sub-Lyapunov [8] exponent of the response system will be negative.

Dynamical interdependence or generalized synchrony implies predictability, and such predictions were described in [4] using local polynomial maps of a driving system to predict the behavior of a unidirectionally coupled chaotic response system. Unfortunately the application of these ideas to experimental systems with arbitrary coupling is not straightforward.

In an experimental setting, where the degrees and directions of coupling between elements are not known *a priori*, we assume that all we can do is to record one or more observable variables from two potentially dynamically linked systems. Our goal is to reconstruct the dynamics as best we can from these observed variables using delay coordinates [5], and then apply a statistic to check for the existence of dynamical interdependence between the two reconstructed systems. If a function exists that maps the values from one system to another, this implies the ability to predict one system through a knowledge of the other. This is the basis of our mutual prediction technique, which provides a measure for both the relative strength and the directionality of the coupling between the two systems. By defining the predictability of each system based on a knowledge of the other system, we derive a measure of dynamical interdependence. In the special case when two systems are unidirectionally coupled, *bidirectional* mutual prediction between their corresponding observable variables implies the existence of generalized synchrony [4,6,7].

Seeking a broader definition for dynamical interdependence in the nervous system has important implications. One of the central questions facing neuroscience today concerns the ''binding problem'' — how the brain integrates separate neural events into perceptions [9]. Traditionally, cross correlation and coherence have been relied upon to correlate neuronal and behavioral activity in spatially disparate portions of the brain [10]. Yet the elements of the brain are inherently nonlinear in that the basic unit of activity is mediated by all or none action potentials, and even synaptic transmission tends to be highly nonlinear [11]. Indeed, it is suggested that the essence of neural computation lies within this inherent nonlinearity [12]. Furthermore, neural activity seems to be incessantly ''noisy'' [13]. Whether some of this noise might be deterministic, perhaps chaotic, has been investigated recently, and there is mounting evidence that a degree of determinism not accounted for by linear models may be observed in neuronal ensembles [14–16]. We therefore postulate that the study of synchrony in the nervous system could be broadened by examining nonlinear coupling. We note that others have recently speculated on whether generalized synchrony occurs in information processing of neural assemblies [7]. To our knowledge, what follows is the first attempt to detect nonlinear coupling or generalized synchrony in a neuronal ensemble.

We chose to study a relatively simple neuronal ensemble — the motoneurons of the monosynaptic spinal cord stretch reflex. The monosynaptic stretch reflex is among the simplest and most accessible of mammalian neuronal ensembles. It is also perhaps the best studied of all mammalian neuronal networks [17,18]. This preparation offers the ability to measure both the firing of multiple individual neurons, and simultaneously measure the population activity in terms of the total number of neurons firing in response to a stimulus. In addition, because of the thickness of the spinal cord and the large size of alpha motoneurons, stable intracellular recordings are achievable over considerable periods of time.

Monosynaptic reflexes are known to be extremely variable [19,20], and in previous work [14] we have demonstrated that in the decerebrate cat spinal cord, a degree of nonlinear predictability was present in the reflex variations that could not be accounted for by linear models. We also demonstrated that the recruitment order of motoneurons could be altered as a function of stimulation frequency, as well as by the recent history of stimulation [20].

In Sec. II, we first describe a zero order mutual predictor and define a method to optimize the different operational parameters. We then discuss the implications of observed mutual predictability in terms of the system's dynamical linkage. The technique of mutual prediction is then applied to unidirectionally coupled maps with identical and nonidentical system parameters in Sec. III A, and the relationship between mutual prediction and generalized synchrony explored through the use of sub-Lyapunov exponents. These results of deterministic driving are then contrasted with random driving of a deterministic numerical system in Sec. III B. We then apply these results to a neuronal ensemble. The experimental preparation is described in Sec. IV A. An analysis of the dynamical interdependence of individual motoneurons and the activity of the motoneuron pool is given in Sec. IV B. A description of the construction of multivariate surrogate data [21] can be found in Appendix A, a discussion of correlation statistics is provided in Appendix B, and a description of sub-Lyapunov exponents can be found in Appendix C.

II. NONLINEAR MUTUAL PREDICTION AND DYNAMICAL INTERDEPENDENCE

We begin with two potentially coupled dynamical systems $\mathcal{X}$ and $\mathcal{Y}$, of which we have no *a priori* knowledge of either their individual dynamics or their dynamical interdependence. For systems $\mathcal{X}$ and $\mathcal{Y}$, we measure time series of observable variables, x_i and y_i $(i=1 \ldots N)$. Since time series from different systems will in general not contain the same range of values, each time series will be normalized as

$$\hat{x}_i = \frac{x_i - \langle x \rangle}{\sigma_{x_i}}$$

and

$$\hat{y}_i = \frac{y_i - \langle y \rangle}{\sigma_{y_i}},$$

where $\langle\ \rangle$ indicates average over i, and σ_{x_i} and σ_{y_i} are the standard deviations of the time series x_i and y_i.

Using the method of time delay coordinate embedding [5], we can reconstruct a chaotic trajectory $\{\vec{x}_i\}$ in an embedding space X using the normalized time series $\{\hat{x}_i\}$ with an appropriately chosen embedding dimension D_x and a lag time L_x,

$$\vec{x}_i = (\hat{x}_i, \hat{x}_{i+L_x}, \ldots, \hat{x}_{i+L_x(D_x-1)}).$$

Similarly, we can reconstruct a chaotic trajectory $\{\vec{y}_i\}$ in an embedding space Y using the normalized time series $\{\hat{y}_i\}$ with an embedding dimension D_y and a lag time L_y,

$$\vec{y}_i = (\hat{y}_i, \hat{y}_{i+L_y}, \ldots, \hat{y}_{i+L_y(D_y-1)}).$$

After [22], we choose the lag time $L_{x,y}$ to be approximately $\frac{1}{4}$ of the decorrelation time of the time series, which is defined as the time it takes the autocorrelation function to decay to $1/e$ of its value at zero lag.

We then ask whether there exists a functional relation Ψ between the reconstructed systems X and Y, i.e.,

$$X \overset{?}{=} \Psi(Y).$$

Such a relation Ψ may be continuous, differentiable (smooth and locally linearizable), and perhaps it has a continuous and/or differentiable inverse. As in [6], we seek a statistical measure of confidence that such a function exists.

For each point $\vec{x}_i$ in the embedding space X, there exists a nearest neighbor of $\vec{x}_i$, $\vec{x}_{nnx_i}$, and their images $\vec{x}_{i+1}$ and $\vec{x}_{(nnx_i+1)}$, respectively. Similarly, for each point $\vec{y}_i$, and its image $\vec{y}_{i+1}$ in Y, there exists a nearest neighbor $\vec{y}_{nny_i}$ and its image $\vec{y}_{(nny_i+1)}$.

After the manner of [4], we may also define a mutual neighbor $\vec{x}_{nny_i}$ of $\vec{y}_{nny_i}$, which is the point in X that bears the index of the nearest neighbor of $\vec{y}_i$. Similarly, there is a mutual neighbor $\vec{y}_{nnx_i}$ of $\vec{x}_{nnx_i}$ in Y. The iterated images of these mutual nearest neighbors are $\vec{x}_{(nny_i+1)}$ and $\vec{y}_{(nnx_i+1)}$, respectively. Figure 1 illustrates these points.

We now incorporate these true and mutual nearest neighbors in a nonlinear mutual predictor. Based on previous work [14,23,24], we will choose the simplest implementation of this predictor—using local *zero order* (constant) maps. While a *zero order* nonlinear predictor checks for the existence of a *continuous* map Ψ between X and Y, a higher order nonlinear predictor could be used to verify the existence of differentiability.

For each index point $\vec{x}_0$ in the embedding space X, we find its k nearest neighbors, $\{\vec{x}^j_{nnx_0}\}_{j=1,\ldots,k}$. With a translation horizon of $H \geqslant 0$ time steps ahead, the prediction is the average translation given by

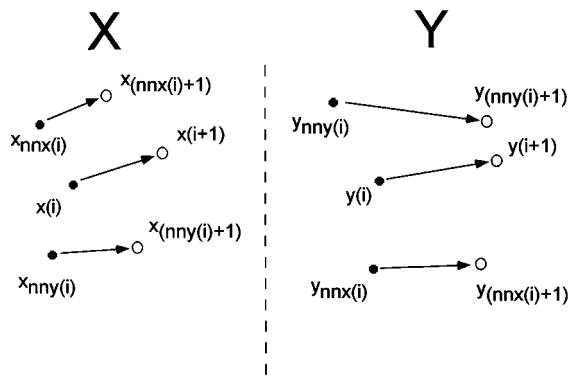

FIG. 1. Illustration of points in two phase space reconstructions, X and Y, from two systems, $\mathcal{X}$ and $\mathcal{Y}$. Each index point, $x_{(i)}$ and $y_{(i)}$, has nearest neighbors in phase space $x_{(nnx_i)}$ and $y_{(nny_i)}$ respectively. Each index point also has a mutual neighbor, a neighbor that uses the time index of the true nearest neighbor of the other system, $x_{(nny_i)}$ and $y_{(nnx_i)}$, respectively. The images (open circles, O) of these points are the iterated values indicated by the arrows in the figure.

$$\langle v \rangle_{nnx(x)} = \frac{1}{k} \sum_{j=1}^{k} \vec{x}^j_{(nnx_0+H)}$$

while the translation of the index point is $\vec{x}_{0+H}$. The difference between the actual and average predicted translation is the prediction error, $\varepsilon_{nnx(x)}$,

$$\varepsilon_{nnx(x)} = |\vec{x}_{(0+H)} - \langle v \rangle_{nnx(x)}|.$$

The prediction error for the mean of the time series, $\varepsilon_{\text{mean}}$, is

$$\varepsilon_{\text{mean}} = |\vec{x}_{(0+H)} - \langle x \rangle|.$$

The normalized prediction error Δ is the discriminating statistic for this method

$$\Delta_{nnx(x)} \equiv \frac{\langle \varepsilon_{nnx(x)} \rangle_{\text{rms}}}{\langle \varepsilon_{\text{mean}} \rangle_{\text{rms}}}$$

where rms indicates root-mean-square. When this normalized prediction error is no different from the error of guessing the mean, Δ will equal 1. This is what one would expect for a time series without nonlinear predictability. On the other hand, if the time series is deterministic, Δ will be less than 1. Source code for this algorithm can be found in [25].

Similarly, we may define a prediction of $\vec{x}_0$ at H time steps ahead based on the mutual nearest neighbors $\{\vec{x}^j_{nny_0}\}_{j=1,\ldots,k}$, such that

$$\langle v \rangle_{nnx(y)} = \frac{1}{k} \sum_{j=1}^{k} \vec{x}^j_{(nny_0+H)},$$

with

$$\varepsilon_{nnx(y)} = |\vec{x}_{(0+H)} - \langle v \rangle_{nnx(y)}|$$

and

$$\Delta_{nnx(y)} \equiv \frac{\langle \varepsilon_{nnx(y)} \rangle_{\mathrm{rms}}}{\langle \varepsilon_{\mathrm{mean}} \rangle_{\mathrm{rms}}}.$$

With two time series, one can define four relevant components of this nonlinear mutual predictor. With $\Delta_{nnx(x)}$ and $\Delta_{nnx(y)}$ defined above, the equations for $\Delta_{nny(x)}$ and $\Delta_{nny(y)}$ are similarly constructed. $\Delta_{nnx(x)}$ and $\Delta_{nny(y)}$ are simply statements of determinism within the individual time series $\{x_i\}$ and $\{y_i\}$, while $\Delta_{nnx(y)}$ and $\Delta_{nny(x)}$ indicate the directionality of prediction between the systems X and Y.

While generalized synchrony between coupled systems $\mathcal{X}$ and $\mathcal{Y}$ implies bidirectional mutual predictability ($\Delta_{nnx(y)}<1$ and $\Delta_{nny(x)}<1$) in the embedding spaces X and Y, only in the case of unidirectionally coupled systems will the inverse be true [4,7]. If the systems $\mathcal{X}$ and $\mathcal{Y}$ are bidirectionally coupled, Takens' theorem [5] guarantees that either x_i or y_i from $\mathcal{X}$ or $\mathcal{Y}$ will be a valid scalar variable for reconstructing the combined dynamics of the coupled system $\mathcal{X}\oplus\mathcal{Y}$ using time delay coordinate embedding. The reconstructed attractors in the embedding spaces X or Y are *equivalent* representations of the same combined dynamics. In other words, by the virtue of the embedding theorem, X and Y will always be predictable from each other with or without generalized synchrony. The requirement for generalized synchrony is stricter. One has to show the existence of a homeomorphic map between the driver $\mathcal{X}$ and the response $\mathcal{Y}$. However, in the reconstructed embedding spaces X or Y, one cannot easily identify the appropriate projections of the combined system $\mathcal{X}\oplus\mathcal{Y}$ onto the original subspaces $\mathcal{X}$ and $\mathcal{Y}$. Thus, in bidirectionally coupled systems, mutual prediction in the reconstructed spaces X and Y does not guarantee generalized synchrony.

On the other hand, if the systems $\mathcal{X}$ and $\mathcal{Y}$ are unidirectionally coupled (i.e., information only flows from $\mathcal{X}$ to $\mathcal{Y}$), then bidirectional mutual prediction in the embedding spaces X and Y does imply generalized synchrony. In a unidirectionally coupled system, the reconstructed attractor in X will represent the dynamics in $\mathcal{X}$ *alone*, while the attractor reconstructed in Y will represent the *combined* dynamics of $\mathcal{X}\oplus\mathcal{Y}$. By Takens theorem again, X will be predictable from Y, since $\mathcal{X}\oplus\mathcal{Y}$ contains all dynamical properties of $\mathcal{X}$ through the one way coupling. Now, if Y is also predictable from X, implying the topological equivalence of the combined system $\mathcal{X}\oplus\mathcal{Y}$ and its projection onto $\mathcal{X}$, then $\mathcal{Y}$ must also be topologically equivalent to $\mathcal{X}$.

In general, the dimensions of the embedding spaces, $D_{x,y}$ required to perform the predictions, true or mutual, are different. Accordingly, we will need to optimize the embedding dimension and the number of nearest neighbors used for each calculation. We will do this by searching for a local minimum of Δ as a function of $D_{x,y}=1,2,\ldots,D_{\max}$ in the one-step prediction error with one nearest neighbor ($k=1$). Then we use this value of $D_{x,y}$ as the number of nearest neighbors is varied, $k=1,2,\ldots,k_{\max}$, until another local minimum of Δ is found. For the following calculations we set $D_{\max}=10$ and $k_{\max}=0.02N$. Ideally, this optimization procedure can be continued until the one-step prediction error falls into a prescribed range, but we have limited the optimization to three steps for each $D_{x,y}$ and k pair because of computational constraints.

III. NUMERICAL STUDIES

A. Coupled identical and nonidentical chaotic systems

As our first simple numerical example showing generalized synchrony between two coupled systems $\mathcal{X}$ and $\mathcal{Y}$, we will use two unidirectionally coupled Hénon maps,

$$\mathcal{X}\begin{cases} x_{i+1}=1.4-x_i^2+0.3u_i \\ u_{i+1}=x_i, \end{cases}$$

$$\mathcal{Y}\begin{cases} y_{i+1}=1.4-(Cx_i+(1-C)y_i)y_i+Bv_i \\ v_{i+1}=y_i. \end{cases}$$

These coupled equations form a *driver* $\mathcal{X}$ and *response* system $\mathcal{Y}$, with the strength of coupling, C, varying from 0 to 1. We will set the coefficient $B=0.3$ for identical systems, and $B=0.1$ for nonidentical systems. The numerical experiments were performed using 1024 time series points x_i from the $\mathcal{X}$ system, and 1024 time series points y_i from the $\mathcal{Y}$ system, sampled following the systems' initial transient responses.

With this driver-response system, we will first demonstrate that mutual prediction gives information regarding the direction of coupling (or the direction of information flow in an experimental system where the underlying equations are unknown). Then we will show that generalized synchrony between the driver and the response system is possible by demonstrating the existence of mutual predictability (in both directions) in certain ranges of coupling values C. Lastly, using a common driving system to drive two identical copies of the response system, we will illustrate the concept of synchronization between two responses driven by a common driver. Three types of numerical experiments will be performed: (1) coupling of identical systems; (2) coupling of nonidentical systems; and (3) stochastic driving of a deterministic system. The statistical significance of our results will be demonstrated using the technique of surrogate data [21] (see Appendix A).

Figure 2 shows plots of x_i versus y_i for identical systems with $C=0.1,\ 0.65$, and 0.9. For nearly identical chaotic systems, sufficient degrees of coupling generate near perfect synchrony [8]. The corresponding prediction errors for these data are shown in Figs. 3(A), 3(B), and 3(C). In Fig. 3, circles represent the prediction errors for the data, and the thin black lines represent the surrogate data predictions (see Appendix A). Notice that the 19 thin lines representing the 19 surrogates form a tight group around the surrogate mean. With the use of 19 surrogates, experimental prediction errors smaller than any of the 19 surrogate predictions have significance (although the actual separation of the experimental results from the surrogate mean in terms of standard deviations of separation—*sigmas*—may not be very substantial). In this figure, the labels $X(X)$, $X(Y)$, $Y(Y)$, and $Y(X)$ stand, respectively, for the delay space reconstructions of X predicted by X ($\Delta_{nnx(x)}$), X predicted by Y ($\Delta_{nnx(y)}$), Y predicted by Y ($\Delta_{nny(y)}$), and Y predicted by X ($\Delta_{nny(x)}$). For each of the four panels in the figure, the optimized values of embedding dimension (D) and number of nearest neighbors (NN) used in the calculations for experimental and surrogate data are indicated. At $C=0.1$, each individual system in X and Y is predictable, indicating determinism in both X and Y. Notice

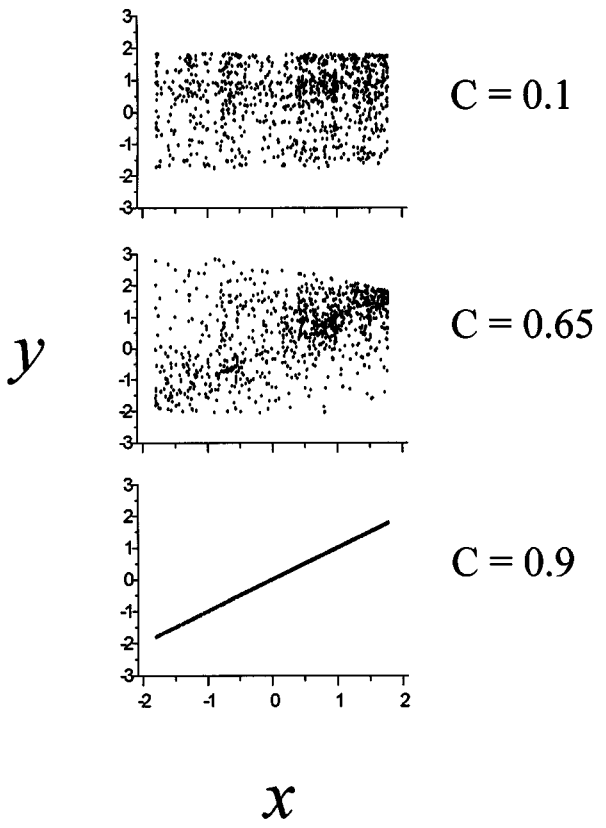

FIG. 2. Plot of x vs y for Hénon equations with identical parameters for various levels of coupling C. For these chaotic systems, sufficient levels of coupling gives perfect linear (identical) synchrony as indicated by the straight line in the panel where $C=0.9$. Units are dimensionless.

that the prediction errors are larger for the response system Y [errors are lower for $X(X)$ than for $Y(Y)$], because $\mathcal{Y}$ is driven by $\mathcal{X}$, and it represents the combined dynamics of both $\mathcal{X}$ and $\mathcal{Y}$. Hence the reconstructed attractor in Y should have a larger dimension than either X or Y alone, and, with a given length of data set, Y should be harder to predict than X.

In Fig. 3(A), it is difficult to see much predictability for the driver X from the response Y for $H \geqslant 1$. Our methodology allows the prediction horizon H to include $H=0$. Calculating mutual nonlinear prediction with $H=0$ is in a sense analogous to the calculation of cross correlation at a lag of zero. Such a calculation would be particularly revealing if the series were very high dimensional or truly stochastic, yet were nonlinearly coupled. Similarly, allowing $H=0$ would help account for the possibility that the systems X and Y are deterministic, yet are sampled too sparsely (the sampling period is greater than the decorrelation time) to pick up the determinism. If we allow $H=0$ for Fig. 3(A), X is clearly predictable from Y for nonzero values of C, as expected (see Fig. 7).

At $C=0.65$ in Fig. 3(B) each individual system is again predictable. Most importantly, at this value of coupling ($C=0.65$), both systems X and Y are mutually predictable indicating the onset of synchrony between the driver X and its response Y [again, the higher dimensional system, $Y(X)$, has larger errors than the lower dimensional system, $X(Y)$]. Lastly, at $C=0.9$, each system X and Y is well predicted through either its true or mutual neighbors, indicating the fully synchronized state of the driver-response system [see also Fig. 2(C)].

Figure 4 shows the difference between the plotted attractors with $B=0.3$ in the $\mathcal{X}$ system versus $B=0.1$ for the $\mathcal{Y}$ system when $C=0$. The equations with the smaller value of B generate an attractor (circles in the figure) that is smaller and fits inside the other one (dots). Figure 5 shows the plots of x_i versus y_i for these nonidentical systems with $C=0.1$, 0.65, and 1.0. For $C=1.0$, the systems are in generalized synchrony, and even for values of $C=1.0$ the plot is not a straight line (identical synchrony), as shown in Fig. 2 for identical systems. This is a generic feature of generalized synchrony for systems with different parameters [4]. Figure 6 shows the prediction and mutual prediction results for $C=0.1$, 0.65, and 0.9 in these coupled nonidentical systems. Similar to the previous case with identical system parameters, at low levels of coupling ($C=0.1$), the driver is predictable from the response, indicating that the system is unidirectionally coupled. At moderate levels of coupling ($C=0.65$), bidirectional mutual prediction is observed, indicating the onset of generalized synchrony between the driver and the response. Finally, at a strong level of coupling ($C=0.9$), each is well predicted through its mutual neighbors, as guaranteed by the existence of generalized synchrony.

An instructive way to visualize the transition to synchrony for these two numerical examples ($B=0.3$ and 0.1) is to plot their mutual predictabilities at $H=0$ as a function of the strength of their coupling C. Figures 7(A) and 7(B) are graphs of $\Delta_{nny(x)}(H=0)$ and $\Delta_{nnx(y)}(H=0)$ for the case $B=0.3$, and Figs. 8(A) and 8(B) are graphs of $\Delta_{nny(x)}(H=0)$ and $\Delta_{nnx(y)}(H=0)$ for the case $B=0.1$. In these graphs, the thinner lines are nonlinear prediction errors calculated from the time series, and the thicker dashed and solid lines indicate the mean and the upper and lower bounds of the surrogates. As a reference to the system's actual behavior in phase space, we also plotted the values of $y_i - x_i$ (with the first 1000 iterates deleted) for each coupling value C in Figs. 7(C) and 8(C). The nonlinear mutual prediction for each coupling value is calculated using 1024 time series points from the driver and response. In order to be consistent in our calculations, all operational parameters are kept fixed with $D=5$, $k=5$, and $L=1$. In both cases, the appearance of bidirectional mutual predictability indicates the occurrence of synchrony (identical in Fig. 7 and generalized in Fig. 8).

Because of the unidirectional coupling, the driver X is always predictable from the response Y as long as the coupling is nonzero in Figs. 7 and 8. With $B=0.3$ (Fig. 7), the transition to synchrony occurs near $C=0.65$. There are large fluctuations in the mutual predictability near this onset value due to intermittent desynchronizations. This on-off intermittency behavior is also evidenced in the y_i-x_i plot in Fig. 7(C). The system finally settles down to the fully synchronized state at $C>0.7$. For nonidentical systems, the transition to synchrony seems to be more complicated. There is no significant bidirectional mutual predictability for C less than 0.2. Then, in the range, $0.2<C<0.5$, $Y(X)$ predictability hovers around the surrogate bounds, and occasionally bursts out with significant mutual predictability. Similar to the iden-

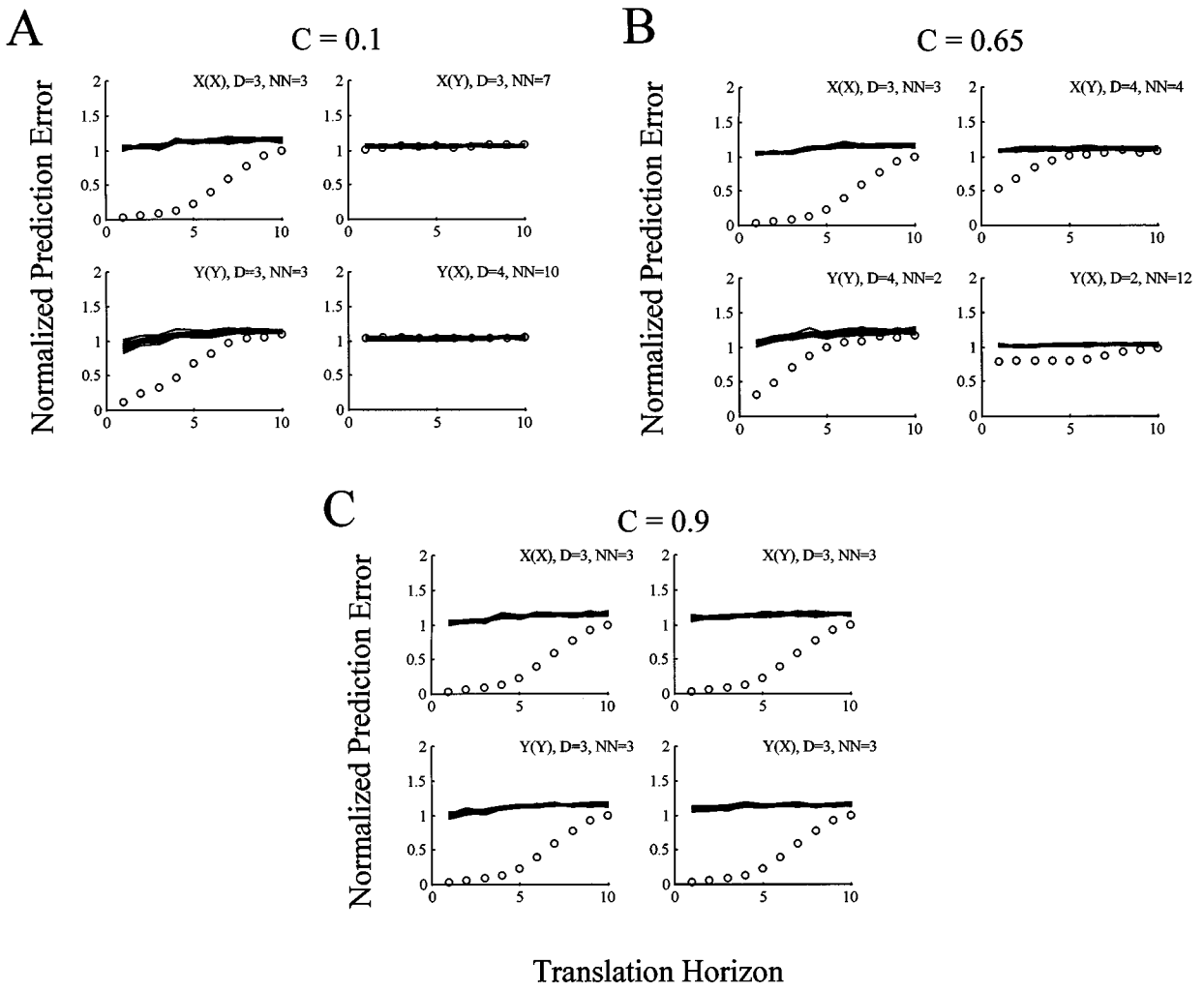

FIG. 3. Nonlinear prediction for identical coupled systems shown in Fig. 2. Four plots are shown for each level of coupling, with the X system as a function of X, $X(X)$, the Y system as a function of Y, $Y(Y)$, X system as a function of mutual neighbors from Y, $X(Y)$; and the Y system as a function of mutual neighbors from X, $Y(X)$. Each of these four types of plots are shown for $C=0.1$ (A), $C=0.65$ (B), and $C=0.9$ (C). Experimental values given by open circles (O), and surrogate values given by thin black lines (−). Nineteen multivariate surrogate pairs are generated from each X and Y pair of experimental data. The optimized values of number of dimensions (D) and nearest neighbors (NN) used in each of the panels are indicated. These values of D and NN are determined from optimizing the one-step prediction error of the experimental data, and the same values are used for the surrogate data calculations. Units for normalized prediction error along the ordinate are dimensionless and normalized to 1, while units for translation horizon along the abscissa are integer iterations of the map. See text for discussion of results.

tical system's case, this on-off synchronization usually characterizes the behavior of a moderately coupled system. Finally, for $C>0.5$, the coupling is eventually large enough to ensure full generalized synchrony.

As discussed earlier, for unidirectionally coupled systems, it is relevant to examine a different concept of synchronization between two responses driven by a common driver. In this case, for sufficiently large coupling, two responses with a common driver will synchronize to each other irrespective of their initial conditions. This state of dynamical interdependence between the responses is characterized by the conditional stability of the response system [7]. Pecora and Carroll [8] first introduced sub-Lyapunov exponents as a measure of this conditional stability (see Appendix C for a detailed description of sub-Lyapunov exponents). In effect, if all sub-Lyapunov exponents of the driven system are negative, then one should expect that all responses with a common driver will asymptotically synchronize to each other. It is important to note that in unidirectionally coupled systems, if the driver and its responses are in generalized synchrony, then two responses with the same driver must synchronize to each other also. Figures 9(A) ($B=0.3$) and 10(A) ($B=0.1$) are plots of the largest sub-Lyapunov exponent calculated from the response system as a function of the coupling C. In order to check if this form of synchronization occurs, we iterated two copies of the response system, $\mathcal{Y}$ and $\mathcal{Y}'$, with the same driver $\mathcal{X}$. Starting with different initial conditions for the response systems $\mathcal{Y}$ and $\mathcal{Y}'$, we plotted the difference y_i-y_i' (with the first 1000 iterates deleted) as a function of C in Figs. 9(B) ($B=0.3$) and 10(B) ($B=0.1$). If the responses synchronize to each other at a particular coupling value, the iterates of the difference y_i-y_i' should be zero. From Figs. 9 and 10, one can see that whenever the largest sub-Lyapunov exponent becomes negative, the difference

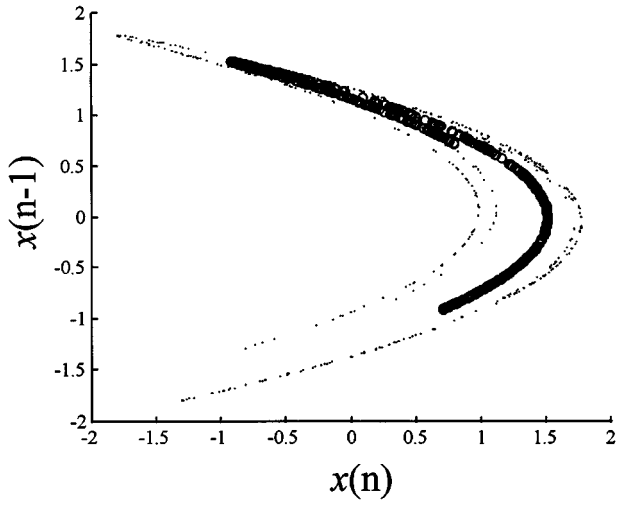

FIG. 4. Illustration of nonidentical Hénon attractors. The black dots (·) correspond to parameter $B=0.3$, and the open circles (O) correspond to parameter $B=0.1$. Units are dimensionless.

between $\mathcal{Y}$ and $\mathcal{Y}'$ is indeed zero. One interesting feature in the case with $B=0.1$ is the existence of two distinct ranges of coupling ($0.18 \lesssim C \lesssim 0.3$ and $C \gtrsim 0.5$) where this type of synchronized response occurs.

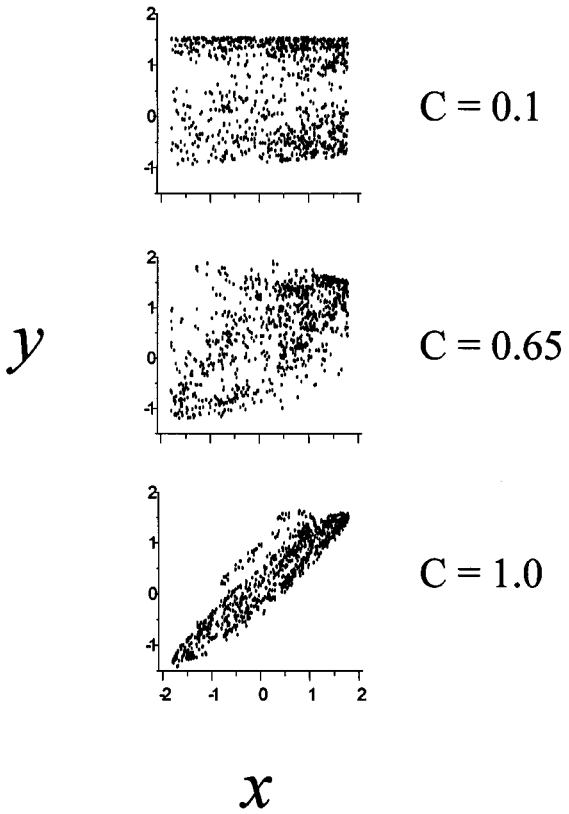

FIG. 5. Plot of x vs y for Hénon equations with nonidentical parameters for various levels of coupling C. In system $\mathcal{X}$, $B=0.3$, and in system $\mathcal{Y}$, $B=0.1$. For these nonidentical chaotic systems, no level of coupling is capable of achieving identical synchrony, and illustrated in the lowest panel is the plot for $C=1.0$ corresponding to generalized synchrony. Units are dimensionless.

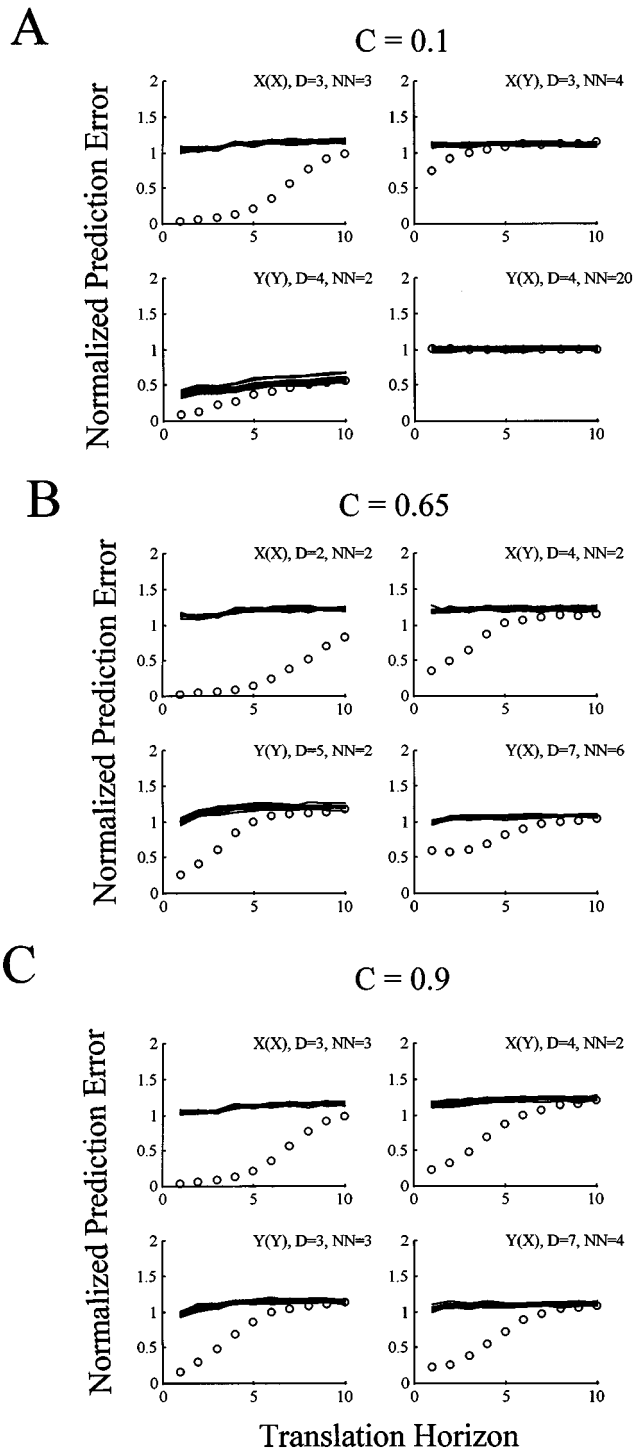

FIG. 6. Nonlinear prediction for nonidentical systems shown in Fig. 5. Four plots are shown for each level of coupling. Symbols, notation, and units are as in Fig. 3. See the text for a discussion of the results.

B. Stochastic coupling of nonlinear systems

To simulate stochastic coupling of nonlinear systems, we start with the iterates x_i of the driving system $\mathcal{X}$ of the nonidentical coupled Hénon maps. We then randomly shuffle the order of the values of x_i, and then iterate the driven system $\mathcal{Y}$ with the randomized sequence of values of x_i. The amplitude distribution of the values from the driving system $\mathcal{X}$ is thus preserved, but any sequence dependent structure or de-

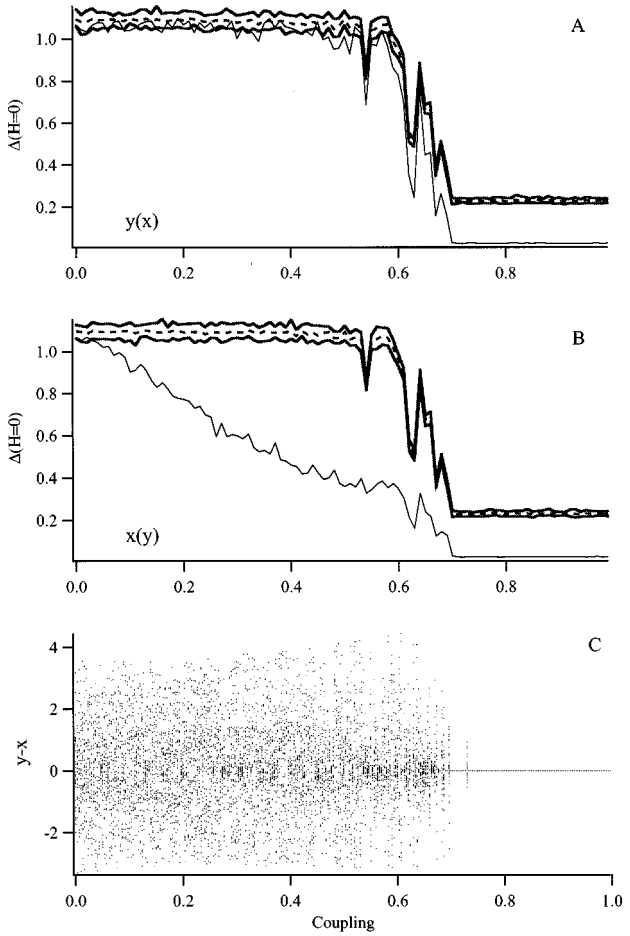

FIG. 7. Normalized mutual prediction errors Δ: (A) $Y(X)$ and (B) $X(Y)$ at $H=0$ as a function of coupling (thin lines). System parameters are identical with $B=0.3$. 1024 data points were used for calculating the mutual prediction errors, and 30 multivariate surrogates were used as a comparison. The thicker dashed and solid lines indicate the surrogate mean, upper, and lower bounds, respectively. All calculations are performed with a set of fixed operational parameters: $D_{x,y}=5$, $k=5$, and $L=1$. A plot of 30 iterates of y_i-x_i (with the first 1000 iterates deleted) are shown as a function of coupling in (C). Units are dimensionless.

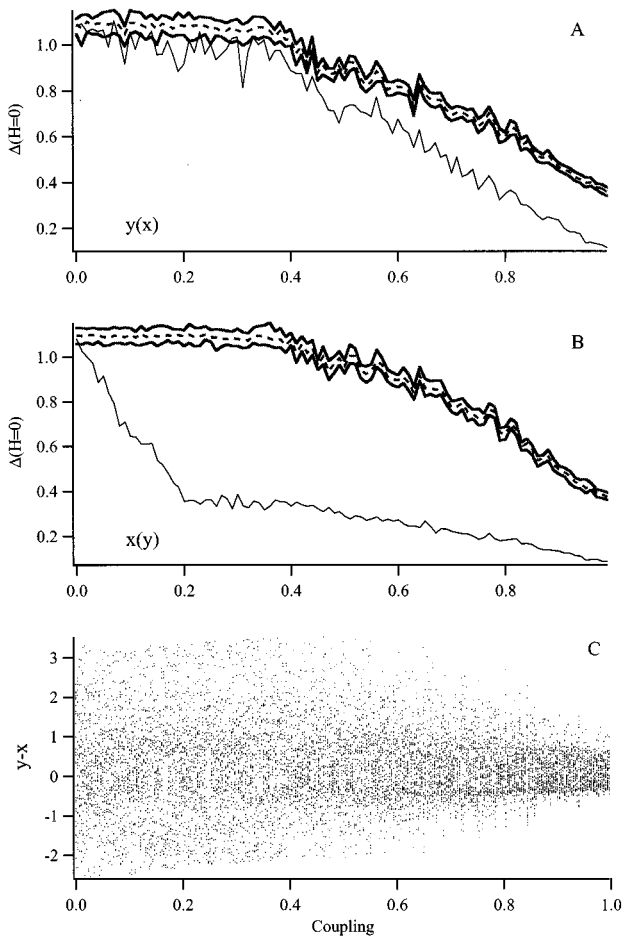

FIG. 8. Normalized mutual prediction errors Δ: (A) $Y(X)$ and (B) $X(Y)$ at $H=0$ as a function of coupling (thin lines). System parameters are nonidentical with $B=0.3$ for the driver and $B=0.1$ for the response. 1024 data points were used for calculating the mutual prediction errors, and 30 multivariate surrogates were used as comparison. The thicker dashed and solid lines indicate the surrogate mean, upper, and lower bounds, respectively. All calculations are performed with a set of fixed operational parameters: $D_{x,y}=5$, $k=5$, and $L=1$. A plot of 30 iterates of y_i-x_i (with the first 1000 iterates deleted) are shown as a function of coupling in (C). Units are dimensionless.

terminism is destroyed. With large enough coupling, it is possible that the random perturbations from the shuffled drive might push the orbit in the response system outside its basin of attractor. In this case, the trajectory of the response system might escape to infinity. Numerically, with 10^6 iterates used in our experiment, all orbits in the response system with $C \lesssim 0.5$ remain bounded. For $C \gtrsim 0.5$, there exist initial conditions in Y such that their orbits escape to infinity after a transient of less than 10^6 iterates.

Figure 11(C) is a plot of y_i-x_i as a function of the coupling C. It appears from this plot that random values of $\mathcal{X}$ have little relation to values of $\mathcal{Y}$. The differences y_i-x_i randomly scatter within the range of possible values for the system. Nevertheless, there exists significant predictability in $Y(X)$ with $C>0.3$, in that the predictability $Y(X)$ is significantly outside of the bounds of the surrogates. Despite this predictability, there exists no bidirectional mutual predictability and thus no generalized synchrony between X and Y. On the other hand, for $C>0.3$, two identical copies of the response systems with different initial conditions and driven by the same random driver $\mathcal{X}$ are able to synchronize with each other, as shown in Fig. 12(B). This occurrence of synchronized responses corresponds to the conditional stability of the response system as indicated by the negative values of the sub-Lyapunov exponents [Fig. 12(A)]. Thus a stochastic driver can, for suitable levels of unidirectional coupling to a response system, show evidence of predictability in the response system through knowledge of the driver $[Y(X)]$, and can even synchronize two response systems, despite the fact that there is no mutual predictability and therefore no generalized synchrony.

IV. MOTONEURON EXPERIMENTS

A. Preparation

The data for this study were collected previously, and the experimental preparation was fully described elsewhere [20].

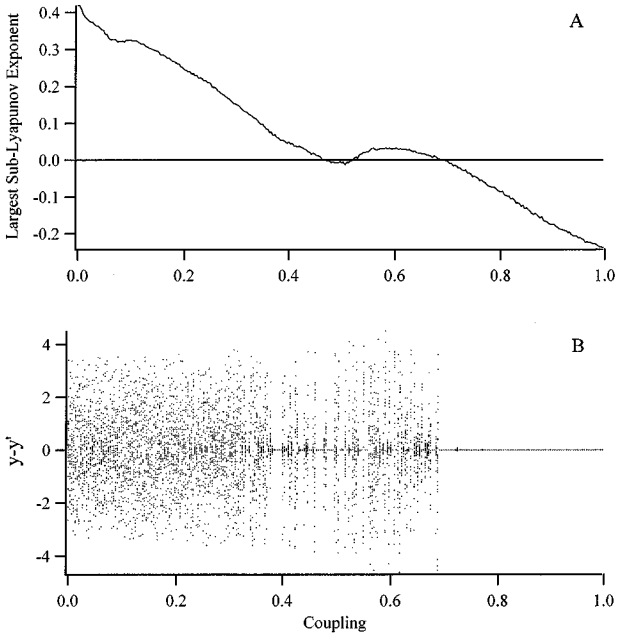

FIG. 9. (A) A plot of the largest sub-Lyapunov exponent in the response as a function of coupling. System parameters are identical with $B=0.3$. 10^6 iterates were used in calculating the sub-Lyapunov exponent. (B) A plot of 30 iterates of the difference between two responses, y_i-y_i' (with the first 1000 iterates deleted), as a function of coupling. Units are dimensionless.

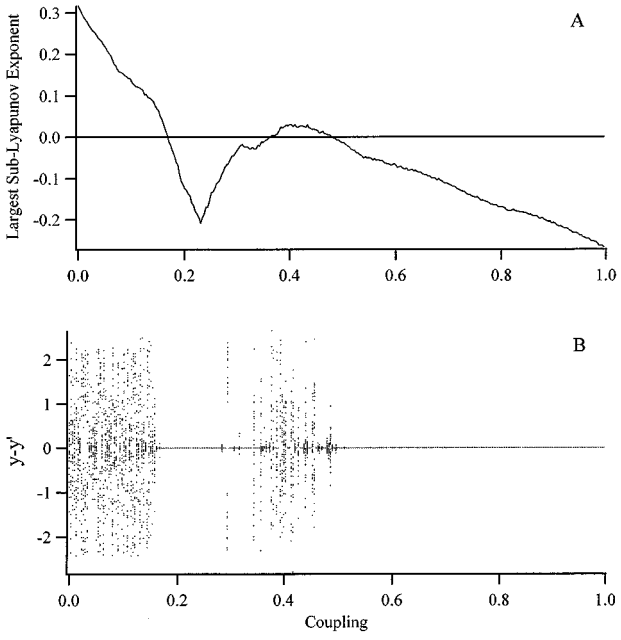

FIG. 10. (A) A plot of the largest sub-Lyapunov exponent in the response as a function of coupling. System parameters are nonidentical with $B=0.3$ for the driver and $B=0.1$ for the response. 10^6 iterates were used in calculating the sub-Lyapunov exponent. (B) A plot of 30 iterates of the difference between two responses, y_i-y_i' (with the first 1000 iterates deleted), as a function of coupling. Units are dimensionless.

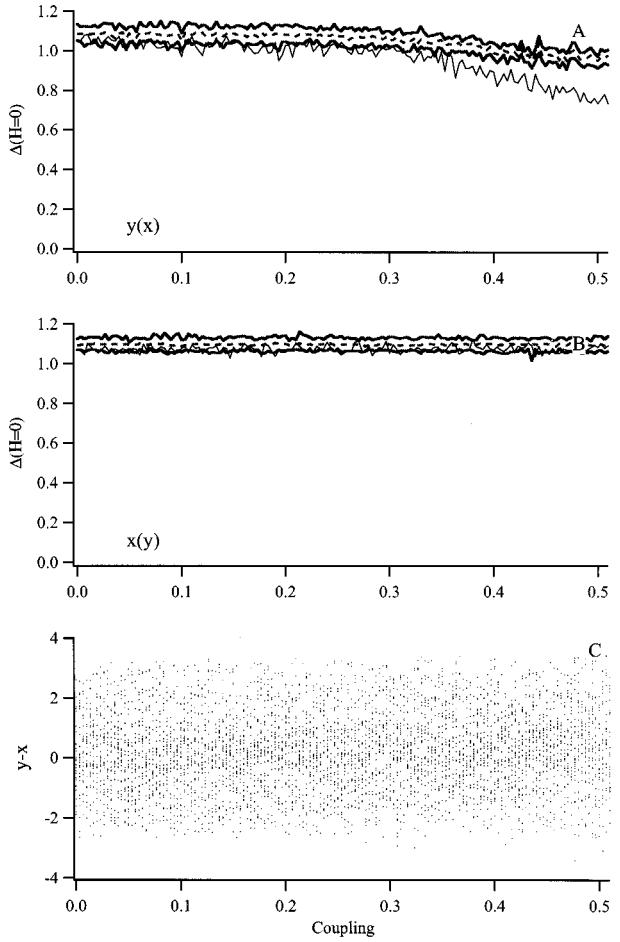

FIG. 11. Normalized mutual prediction errors Δ: (A) $Y(X)$ and (B) $X(Y)$ at $H=0$ as a function of coupling (thin lines). The nonidentical response system ($B=0.1$) is driven with a shuffled driver. 1024 data points were used for calculating the mutual prediction errors, and 30 multivariate surrogates were used as comparison. The thicker dashed and solid lines indicate the surrogate mean, upper and lower bounds, respectively. All calculations are performed with a set of fixed operational parameters: $D_{x,y}=5$, $k=5$, and $L=1$. A plot of 30 iterates of y_i-x_i (with the first 1000 iterates deleted) are shown as a function of coupling in (C). Units are dimensionless.

In brief, four cats were anesthetized, and the blood pressure and temperature maintained within physiological limits. A precollicular postmammillary transection of the midbrain was performed and the spinal cord was exposed.

In the leg the nerves to the medial gastrocnemius (MG), lateral gastrocnemius (LG), soleus (S, often combined with LG as LGS), and posterior biceps and semitendinosus (PBST) muscles were placed on fine platinum bipolar electrodes for stimulation. Muscles were pharmacologically paralyzed to prevent movement artifacts, and the proximal ends of the cut last lumbar (L7) and first sacral (S1) spinal cord ventral (motor) roots were placed on bipolar platinum recording electrodes. Thus a reflex arc with one synapse (monosynaptic) was isolated, from muscle nerve sensory fibers to the output motoneurons from the spinal cord.

Constant voltage 50-μs square wave stimuli were applied to muscle nerves at a frequency of 2 Hz. The intensity of the stimulation was adjusted to yield just supramaximal group-I fiber responses (the large sensory nerve fibers that participate

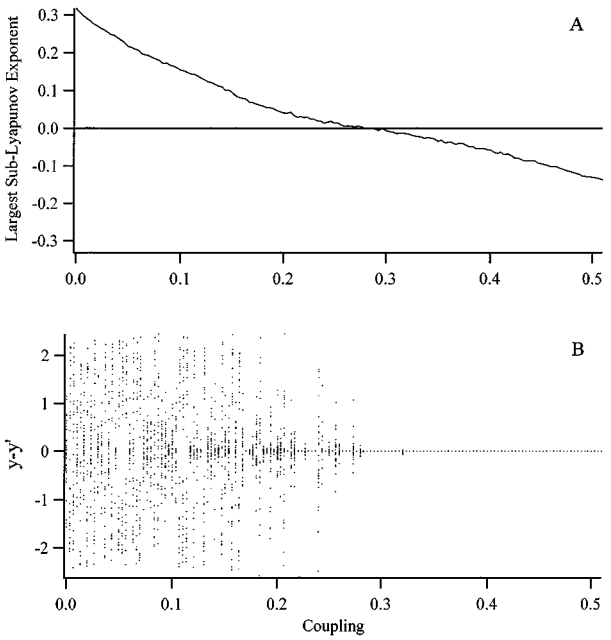

FIG. 12. (A) A plot of the largest sub-Lyapunov exponent in the response as a function of coupling. The nonidentical response system ($B=0.1$) is driven with a shuffled driver. 10^6 iterates were used in calculating the sub-Lyapunov exponent. (B) A plot of 30 iterates of the difference between two responses, y_i-y_i' (with the first 1000 iterates deleted), as a function of coupling. Units are dimensionless.

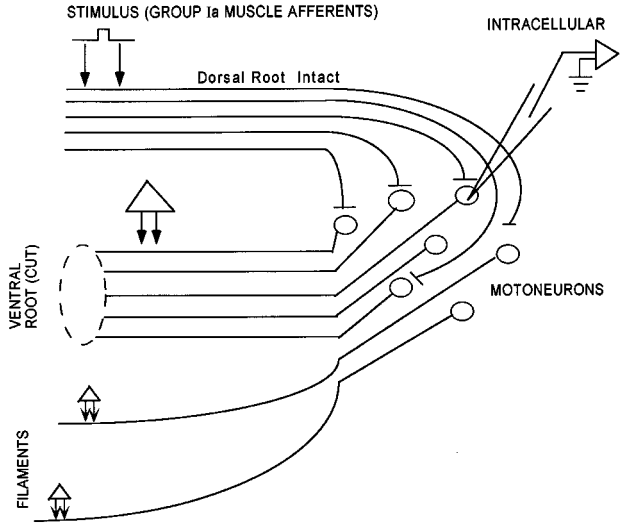

FIG. 13. Schematic of the experimental preparation. Periodic square wave stimuli were applied to an isolated motor nerve containing group Ia afferents which monosynaptically activate α—motoneurons. The axons of the motoneurons pass into the efferent ventral root. Measurements of the electrical monosynaptic reflex were made from the bulk of the cut ventral root, the integrated amplitude of which reflects the number of neurons discharging [28]. Fine filaments from the ventral root were dissected from the bulk of the root, until single motoneuron discharges were detected within the filament. In some experiments, intracellular recordings of EPSP's were made simultaneously with the unit and reflex measurements. Not shown are the dense interneuonal connections within the motoneuron network (''pool''), nor the extensive branching of the afferent fibers so that each one synapses with nearly all of the motoneurons within the pool.

in the monosynaptic reflex) as measured by the cord dorsum potential (recorded with a fine platinum ball placed on the surface of the spinal cord). We attempted to evoke monosynaptic reflexes with single stimulus volleys delivered to MG, LG, and *S*, or PBST muscle nerves. However, for some of the experiments it was necessary to use two stimulus volleys to evoke a measurable monosynaptic reflex (4-ms interval between paired volleys, pairs delivered at 2 Hz); when the response to the second volley was analyzed, special attention was given in these cases to eliminate reflex series showing any detectable response to the first volley.

Recordings were stored digitally and analyzed with LabView2 (National Instruments, Inc.), or Datapac II (Run Technologies, Inc.). The implementation of algorithms to test for autocorrelation, cross correlation, and mutual prediction was performed with MatLab (The MathWorks, Inc.) or C. In the analysis of these data, time windows were set to incorporate the positive deflection of the monosynaptic reflex potential. These recordings were made from ''crushed end'' ventral roots in order to remove biphasic and triphasic components. Baseline potential recordings just before the monosynaptic reflex were subtracted to give the absolute voltage changes recorded at the time of the reflex, and the monosynaptic reflex deflections were integrated during a time window of 1–2 ms.

Fine filaments were teased from the ventral root showing the largest monosynaptic reflex, and the filaments were subdivided until single motoneuron (unit) discharges to a selected muscle nerve were detected. One to three such ''single fiber'' filaments were placed on separate fine bipolar platinum electrodes for simultaneous recording with the monosynaptic reflex from the bulk of the ventral root. A schematic of the experimental preparation is shown in Fig. 13. In order to study how the variability in the firing frequency of such units contributes to the dynamics of the population, we eliminated from this study units with firing probabilities greater than 0.95 and less than 0.05 (the firing probability is the probability that a motoneuron will fire in response to a single stimulus).

Intracellular recordings were made with glass micropipettes (1.0–2.5 MΩ) filled with 3-M potassium acetate or 100-mM QX314 (Alomone Laboratories, Jerusalem) in 2-M potassium acetate to suppress sodium spikes [27]. Figure 14 illustrates an example of simultaneously measured cord dorsum potential (CDP), intracellular excitatory postsynaptic potential (EPSP), a single fiber unit response (UNIT), and monosynaptic reflex (MSR). Shown in the figure is the time window (dotted lines) defined by the MSR duration during which the MSR is integrated and the unit responses corresponding to that MSR are identified. Since the synaptic currents precede the MSR, the time window (dotted lines) shown for EPSP integration is different.

B. Experimental results

Applying the mutual prediction technique to the data from our motoneuron experiments, we will illustrate the dynamical relationship between single motoneurons and the monosynaptic reflex amplitude. The reflex is stimulated periodically, and recordings from single motoneuron axons from the

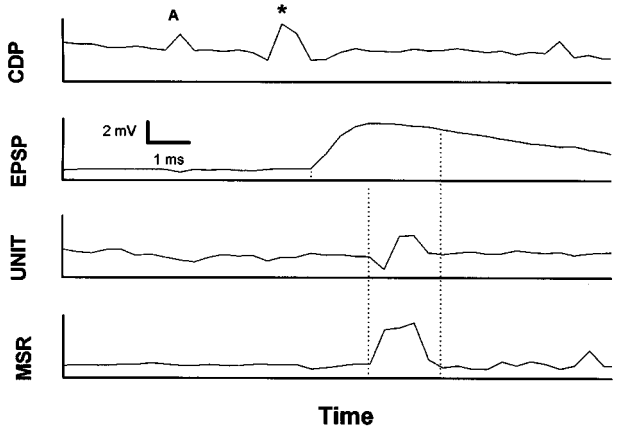

FIG. 14. Sample of raw data recorded from an experiment. The cord dorsum potential (CDP, indicated by an asterisk) reflects the incoming afferent discharge and is recorded from the surface of the spinal cord with a small platinum ball electrode. The stimulation artifact is indicated (A). The EPSP is recorded from an intracellular electrode within a single motoneuron. The UNIT response is from a dissected filament and reflects the action potential from a single motoneuron. The monosynaptic reflex (MSR) is the compound action potential of the single units, and the integrated MSR is proportional to the number of units discharging in response to a stimulus. The dotted lines represent the windows of the monosynaptic reflex, and are discussed further in the text. The calibration bars give the scale of the ordinate and abscissa in mV and ms, respectively, for each panel in the figure.

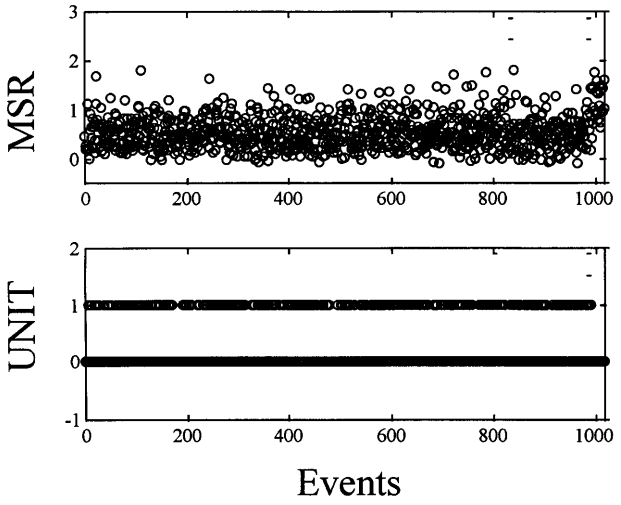

FIG. 15. Sample of two simultaneous time series. In the upper panel are integrated values of monosynaptic reflexes (MSR), and the lower panel reflects whether a single unit (UNIT) fired (1) or not (0) during each MSR. Unit firings and failures are frequent, and there is much overlap in the plotted points in the lower panel. The abscissa records the number of events analyzed, and the 1000 points recorded correspond to 500-s elapsed time (the stimulation frequency is 2 Hz). The ordinate is in arbitrary units of voltage for MSR.

same motoneuron pool are made simultaneously with the population discharge. Thus this experiment captures the instantaneous activity of a population of coupled neurons, and samples several of the individual neurons at the same time. We examine the interactions not only of the individual motor units with the population of the motoneurons from the pool, but also study the interactions between individual units. For some experiments, simultaneous sampling of the synaptic currents (EPSP) from individual motoneurons was also obtained, and the degree of nonlinear coupling between the EPSP's and both the unit and population responses was determined.

Figure 15 shows a pair of simultaneously measured time series of a MSR and a unit response. Each monosynaptic reflex value reflects integration over a 1–2-ms time window (see Fig. 14), and these values are proportional to the number of neurons discharging within the motoneuron pool at one time [28]. The unit response is a 1 or 0, depending on whether the unit fired during the time window defined by the duration of the MSR. Firings and failures of the unit response are frequent, reflected in the overlapping of 1's and 0's in Fig. 15.

Figure 16 demonstrates the linear correlations for this MSR and a single unit response. The linear correlations of each time series are expressed as autocorrelation, and the dotted lines represent ± 2 standard deviations assuming a null hypothesis that no significant autocorrelation exists (see Appendix B). The lowest tracing in the figure illustrates the linear cross correlation between these two time series, and the dotted lines again represent ± 2 standard deviations. For these two time series, although there is no significant autocorrelation for either series, there is significant cross correlation at a lag equal to 0.

Figure 17 plots the nonlinear prediction and mutual prediction of these two time series, plotted as open circles. Shown are four plots illustrating the normalized prediction errors of the MSR as a function of the MSR, MSR(MSR),

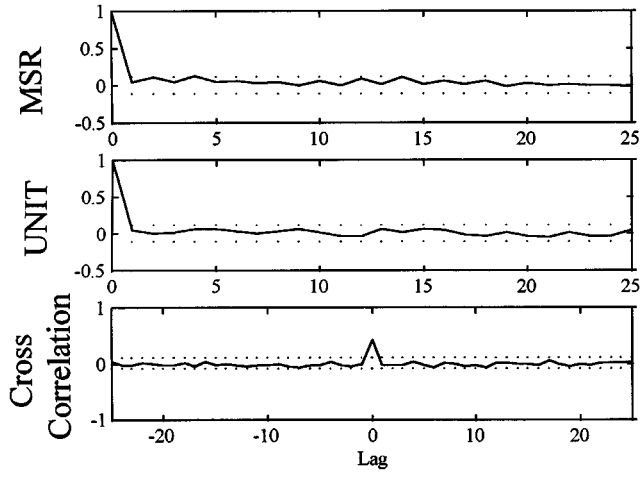

FIG. 16. Shown for the data in Fig. 15 are the autocorrelation of the MSR and UNIT. One lag is equivalent to 500 ms. The dotted lines represent 95% confidence intervals that the autocorrelations are different from white noise (see Appendix B). The lower panel shows the cross correlations for these time series. The dotted lines here represent the 95% confidence intervals that these cross correlations are produced at random for a given lag. Note that the axis of the time lags are different—autocorrelations are presented as one-sided functions for positive lags only, while cross correlations are shown for both positive and negative lags. Units of all ordinates are dimensionless.

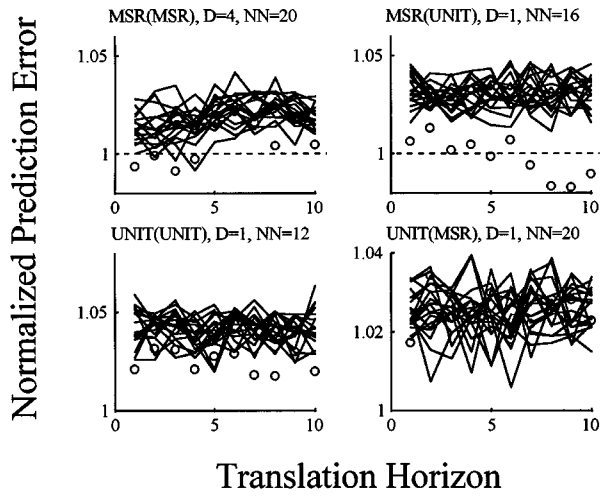

FIG. 17. Nonlinear prediction for the data shown in Figs. 15 and 16. Shown are four plots illustrating the normalized prediction errors of the MSR as a function of the MSR, MSR(MSR), MSR as a function of the unit response, MSR(UNIT), the single unit as a function of itself, UNIT(UNIT), and the unit as a function of the MSR, UNIT(MSR). The prediction errors are normalized so that a prediction error of 1 or greater is no better than guessing the mean value of the time series. Experimental values given by open circles (O), and surrogate values given by thin black lines (−). As discussed in the text, the MSR has nonlinear predictability, MSR(MSR), and mutual predictability through consideration of the unit response, MSR(UNIT). This unit had no nonlinear predictability, UNIT(UNIT), and no mutual predictability UNIT(MSR). A dotted line (- - -) at 1 is shown in the upper panels, below which predictability is significant. Abscissae are in units of the period of stimulation, each translation horizon corresponding to 0.5 s. Ordinate units are dimensionless.

MSR as a function of the unit response, MSR(UNIT), the single unit as a function of itself, UNIT(UNIT), and the unit as a function of the MSR, UNIT(MSR). Nineteen multivariate surrogate data sets were generated for each pair of time series, as described in Appendix A, and their surrogate results were plotted as solid lines without symbols. These surrogate data sets preserve both the autocorrelation of each individual data set, and the cross correlation. The prediction errors for both the experimental and surrogate data are normalized so that if the prediction is no better than guessing the mean (or worse), the values will be $\geqslant 1$. Only values less than 1 and less than any of the surrogate values for a given translation horizon are considered significant. For this MSR and the single unit, the MSR had nonlinear predictability [MSR(MSR)], as well as mutual predictability [MSR(UNIT)]. The existence of mutual predictability indicates that the MSR could be predicted through knowledge of the unit firing, beyond the predictability inherent in their linear correlations. On the other hand, the unit demonstrated no nonlinear predictability [UNIT(UNIT)] of its own, and no mutual predictability in that the unit could not be predicted through knowledge of the MSR [UNIT(MSR)]. Unlike cross correlation, mutual prediction demonstrates directionality of coupling.

Similar computations were performed for each of 69 pairs of data from three experiments where the quality of the simultaneous time series permitted this sort of comparison. Figures 18(A), 18(B), 18(C), and 18(D) illustrate the dynamical coupling between the MSR, units, and when available, intracellular data for all 69 pairings. On the left side of these figures, the linear correlations are diagrammed, and on the right side the nonlinear correlations are given in terms of predictions that the linear correlations could not account for. Symbols used are MSR: a–e for UNIT's, and IC for intracellular responses. For each symbol, statistically significant autocorrelation and nonlinear prediction are indicated by a superscript + (and lack of significance as a superscript -), linear cross correlation by a solid line, and mutual prediction by a directional arrow. For pairs of data that showed no mutual predictability at $H>1$, computations were reoptimized for $H=0$, and significant mutual predictability at $H=0$ only is indicated with dashed arrows. At the far right of these figures, the specific motoneuron pool under study is indicated (MG, PBST, etc.).

Each of these diagrams illustrate the flow of a given experiment, from top to bottom. Each of the results, indicated by the linkages of MSR, a, b, c, d, e, and IC, are determined from time series recorded at 2 Hz. In between each 2-Hz recording period, different experimental manipulations were performed, as indicated by dotted lines (- - -) with embedded comments: a period of higher-frequency stimulation (10, 50, and 100 Hz), different motoneuron axons were substituted on the recording electrodes, a different peripheral nerve was used for stimulation (e.g., MG changed for PBST), or peripheral nerve conditioning was turned on and off [20]. The longest dotted lines correspond to a transection of the spinal cord, thus physically isolating the lumbar motoneuron pools (spinalization). Detailed descriptions of the physiology of conditioning and frequency changes on motoneuron physiology can be found in [20], and a detailed discussion of the dynamics of MSR's before and after sectioning the spinal cord can be found in [14].

In the decerebrate state [upper portions of Figs. 18(A) and 18(B)], all but one of the MSR recordings demonstrated strong linear correlation, and at times there was a strong element of nonlinear predictability in these decerebrate MSR series (as fully discussed in [14]). These significant linear and nonlinear properties of the time series are indicated in the figure by superscripted plus signs (MSR^{+}).

The network diagrams in Fig. 18 demonstrate that nonlinear coupling can frequently be observed in a neuronal ensemble between units, between units and the population, and between units and the intracellular EPSP's. Cross correlations are at times observed when no nonlinear coupling is seen, between units and the MSR, and between the EPSP's and units or MSR. The converse of this, nonlinear correlation without linear cross correlation, is also observed between the units and the population or the EPSP. One way mutual prediction is seen, between units and MSR or EPSP, and even between units themselves. Bidirectional mutual prediction is observed only between units and the population (MSR).

Several specific examples are instructive. In the top row of Fig. 18(A), note that the MSR has a significant linear correlation (+), but the unit a does not (-). Nevertheless, there is a significant cross correlation between this MSR and the unit. Both the MSR and unit have no nonlinear predictability nor nonlinear correlation. Following exposure to 50-Hz stimulation, the system goes into the posttetanic state

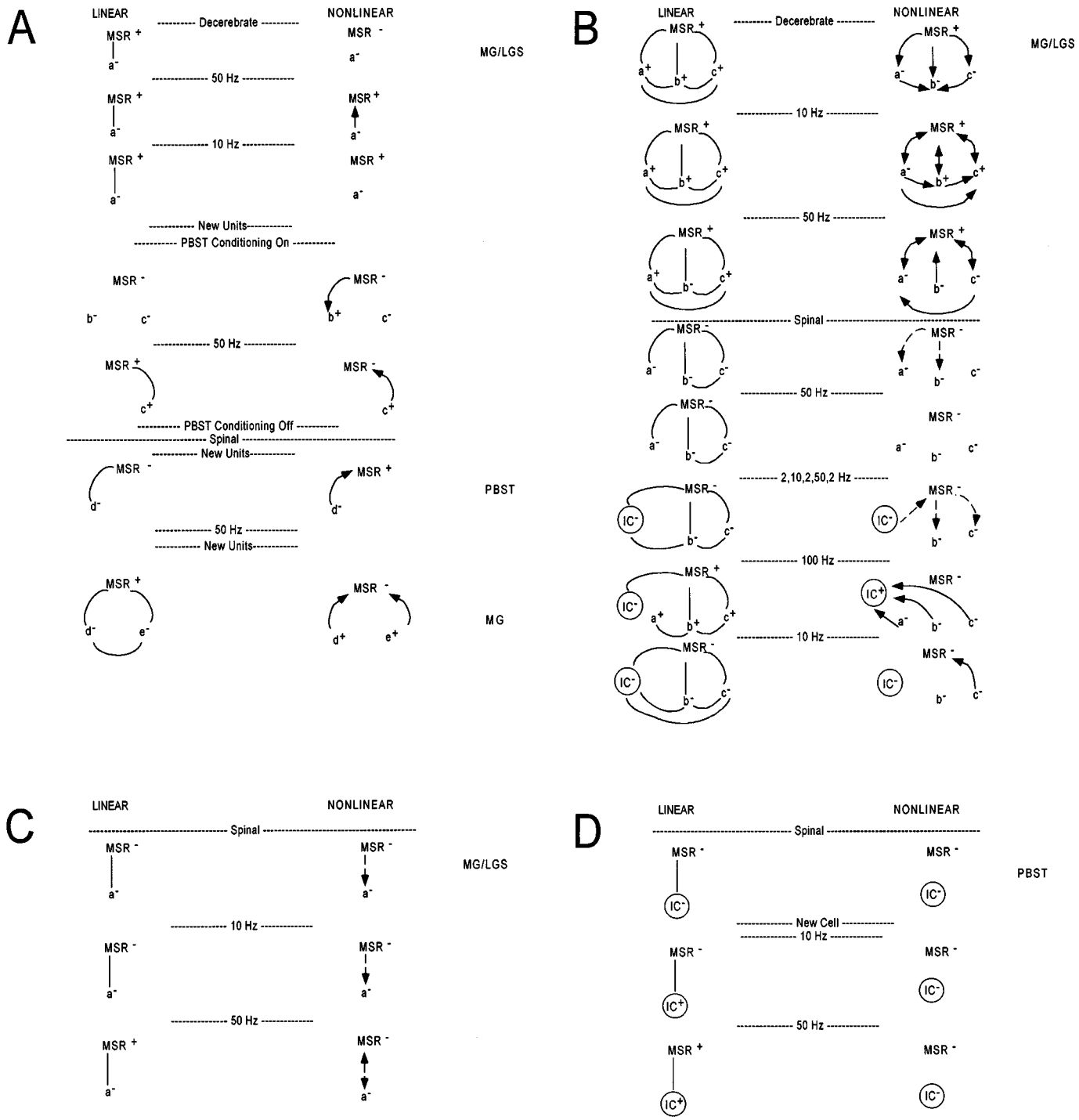

FIG. 18. Network figures for linear (autocorrelation and cross correlation) and nonlinear correlations for 69 pairs of time series representing monosynaptic reflexes (MSR), single unit responses (a, b, c, d, and e), and, when available, intracellular EPSP data (IC). The left hand columns indicate the results of the linear analysis, and the right columns the nonlinear analysis. The muscle nerve stimulated (and therefore the particular motoneuron pool under study) is indicated at the far right of each panel (MG, LG, and PBST — see Sec. IV A). Statistically significant autocorrelation, or significant nonlinear prediction not accounted for by the autocorrelation, is indicated by a superscripted plus sign, and the absence of such correlation by a superscripted minus sign. Statistically significant cross correlation is indicated by a solid line (—), and significant mutual nonlinear prediction by a directional arrow (→). For data where mutual prediction is only seen for $H=0$, the directional arrow is dashed. The time series were collected before and after various experimental manipulations, and these events are commented upon in between rows (time proceeds downward in these figures). Although various stimulation frequencies as indicated were applied in between collecting the time series under study, all the time series analyzed here were collected at 2 Hz. Panel (B) represents an experimental sequence where the units a, b, and c were the same throughout the experimental manipulations. Panel (C) shows data from the same experiment in panel (B), but the units are different.

(an increased amplitude of EPSP's with an increased probability of unit responses, and an increase in MSR amplitude following high frequency stimulation). Although the linear properties are unchanged, there now appears to be nonlinear predictability in the MSR, but not in the unit. Nonlinear mutual prediction of the MSR also appears through a knowledge of the unit. The converse is not true—the MSR does not nonlinearly predict the unit. This mutual prediction reveals a functional coupling that is fleeting; following a period of 10-Hz stimulation, the nonlinear coupling is no longer apparent.

Now look at the fourth row of Fig. 18(A), recorded after new units were placed on the recording electrodes and while PBST conditioning was turned on. Here a MSR and two units *b* and *c* demonstrated no linear properties. Nevertheless, there exists significant nonlinear predictability of unit *b* (+), and furthermore, there is mutual nonlinear predictability of unit *b* through knowledge of the MSR. Note further that the MSR has no detectable linear or nonlinear predictability—it is stochastic. *Thus this MSR and the unit demonstrate a nonlinear functional relationship that would have remained undetected with traditional linear methods. In addition, this MSR and unit demonstrate what appears to be an example of mutual prediction resulting from stochastic driving of a deterministic system at moderate levels of coupling, as predicted in Sec. III B.*

The fifth row in Fig. 18(A), following 50-Hz stimulation, again shows changes in the posttetanic state. The unit *b* is no longer detectable. Linear cross correlation now emerges, as does nonlinear correlation, between unit *c* and the MSR. This functional coupling would therefore have been detected by linear analysis, but the nonlinear component of the coupling would not have been appreciated.

Although bidirectionally coupled systems may exhibit generalized synchrony, as discussed above, we have no straightforward way of identifying such synchrony from delay variables at present. The complexity of the spinal motoneuron pool dictates that we cannot be sure that we know the direction of coupling *a priori*. Nevertheless, we can search for evidence of unidirectional coupling through unidirectional mutual prediction, and then see if a perturbation of the system introduces bidirectional mutual predictability. Examination of the network figures in Fig. 18 shows examples where unidirectional mutual prediction from MSR to units was converted to bidirectional mutual prediction following a perturbation, generally following high frequency stimulation, and our interpretation of this is that we may indeed be observing the conversion of unidirectionally coupled systems to generalized synchrony in these cases. In Fig. 18(B), in the decerebrate state in the first row, note that there is unidirectional nonlinear coupling evident in the prediction of the unit behaviors (*a*, *b*, and *c*) from the MSR. Following 10-Hz stimulation, note the conversion of the nonlinear prediction to bidirectional between these same elements. *This may represent an example of the induction of generalized synchrony as the effective coupling strength of these elements was increased in the posttetanic state.*

Between the third and fourth rows in Fig. 18(B), sectioning the spinal cord (spinalization) was performed without losing the unit recordings. This isolated the motoneuron pool under study, removing the influence from higher in the spinal cord and from the brain stem. Following spinalization, both autocorrelation and nonlinear prediction were almost entirely lost (as previously reported in [14]), but many of the cross correlations were preserved. The two dashed arrows in the fourth row of this figure indicate that prediction was seen only for $H=0$ for these elements (MSR predicting units *a* and *b* only). Although nonlinear coupling appeared weak following spinalization, strong $H>0$ mutual prediction returned following high frequency (100 Hz) stimulation, again during posttetanic potentiation. In the third row from the bottom of Fig. 18(B), there is no nonlinear predictability between the units (*b* and *c*) and the intracellular EPSP amplitude (IC). Following 100-Hz stimulation, there emerges evidence of nonlinear coupling in that the units now predict the intracellular response, even though the units themselves have no nonlinear predictability and there is no linear cross correlation between the units and the intracellular response. In the bottom row of Fig. 18(B), following a period of 10-Hz stimulation, the nonlinear relationships again change. Although the units no longer nonlinearly predict the intracellular response (unit *a* was lost), unit *c* now mutually predicts the MSR, even though both unit *c* and the MSR have no nonlinear predictability themselves. The results in the lower part of Fig. 18(B) correspond to the same experimental data as detailed in the raster plots in Fig. 7 from [20].

In Fig. 18(C), the top row suggests that for this unit and the MSR, there was significant cross correlation without autocorrelation, and evidence of unidirectional nonlinear prediction for $H=0$. *Note that after 50-Hz stimulation, the nonlinear prediction is converted to bidirectional, again highly suggestive that generalized synchrony is induced.*

V. DISCUSSION

These results demonstrate that there is a wide variety of linear and nonlinear coupling among the network of motoneurons generating a monosynaptic reflex. The coupling is quite fluid as a function of time, and changes in experimental conditions. Although some of these couplings would be detected with linear cross correlation, others would not. Since neurons are floridly nonlinear in their action potential generation and synaptic transmission, we are not surprised to identify nonlinear coupling between neurons. The important point is whether such couplings can predict or confirm functional relations between neurons that previous tools could not. Our data suggest that this is so, and methods such as presented here offer a broader understanding of dynamical interdependence in a neuronal network than previously possible.

Although several recent studies suggested both geometrical [4] and statistical [6] approaches to the detection of generalized synchrony, we focused on mutual prediction for neural data. We set up our prediction approach so that the choice of drive and response system need not be known *a priori*, and that knowledge of coupling strength and information flow in a system may be inferred from the results. In addition, our method permits the use of prediction without time lag ($H=0$), and this can significantly improve the identification of coupling in our data.

Although our findings are highly suggestive, we lack the ability to prove the existence of generalized synchrony in

networks such as these where the coupling may be bidirectional. Our best examples are those that started out with evidence of unidirectional mutual prediction only, and changed to bidirectional prediction following an increase in apparent coupling strength after high frequency stimulation (during posttetanic potentiation). One possibility in these experiments is that following high frequency stimulation there emerged true bidirectional coupling. For bidirectionally coupled systems, using delay coordinate embeddings, nonlinear coupling but not generalized synchrony is proven by mutual prediction. Future work to develop our theoretical tools to handle synchrony in bidirectionally coupled experimental systems would be of significant value.

The numerical simulations presented in Sec. III B predicted that driving a nonlinear system with a stochastic signal might reveal mutual prediction, if the coupling levels were moderately strong. This type of coupling was identified within the motoneuron pool in Sec. IV B. Stochastic driving of a deterministic system is poorly categorized by present concepts of generalized synchrony, and further theoretical work in this area would be useful. Nevertheless, these findings provide further evidence that neurons are deterministic nonlinear elements, and perhaps in some sense we may view neurons as nonlinear equations wrapped in protoplasm.

Stochastic resonance was recently experimentally demonstrated in neural networks from mammalian brain [29]. In recent numerical work, aperiodic stochastic resonance was quantified in a neuronal model using a measure of linear correlation [30]. Nonlinear methods such as mutual prediction may form a more powerful approach to answer the question of whether an arbitrary input signal is reflected in the output of a nonlinear system, and could be applied to stochastic resonance data. Whether generalized synchrony may exist in the context of stochastic resonance is an open question for now.

Much interest has been generated in recent years concerning the so-called 40-Hz oscillations in the brain [9]. Of major interest is how such oscillations may synchronize neurons to accomplish an information processing task. Nonlinear mutual prediction and generalized synchrony allow one to take a much broader view of synchrony than simple phase locking. The methods presented here, which are not restricted to motoneurons, open up widely the question of where in the nervous system identifying nonlinear dynamical interdependence or even generalized synchrony could identify new functional relations among neurons.

Our experiments were limited by constraints imposed by the study of motoneuron monosynaptic reflexes. Such reflexes must be studied as input-output relations only, although the simplicity of this neuronal network lent itself well to establishing the existence of neural nonlinear coupling and probably generalized synchrony. We are keen to study continuous time data from autonomously firing neuronal ensembles and their single units (in systems such as used in [15,16]). Indeed, we anticipate that the methods presented here can be readily extended to large scale study of the cerebral cortex, using either traditional electrode or newer optical techniques.

ACKNOWLEDGMENTS

We thank L. Pecora, E. Ott, and C. Grebogi for their helpful discussions. S.J.S. received support from National Institutes of Mental Health Grant No. 1-R29-MH50006-04 and the Children's Research Institute, and S.J.S. and P.S. received support from United States Office of Naval Research Grant No. N00014-95-1-0138. We gratefully acknowledge the support of the Keck Foundation for computing facilities, the granting of a perpetual site license from the MathWorks, Inc., and the contribution of software from Manugistics, Inc.

APPENDIX A: MULTIVARIATE SURROGATE DATA

Surrogate data are models of experimental data based on the null hypothesis we wish to reject (e.g., that the data are explained by a linear stochastic model with linear coupling). We draw upon the work of [21] to construct multivariate surrogate data for our experimental data. In this method, linearly stochastic time series pairs x_i' and y_i' are generated from the experimental time series pairs $\hat{x}_i$ and $\hat{y}_i$, with the linear correlations within each component time series and the cross correlation between them preserved. Such surrogate data have no nonlinear properties.

The cross correlation $r_{xy}(\tau)$ of $\hat{x}_i$ and $\hat{y}_i$ is

$$r_{xy}(\tau)=\langle \hat{x}_i \hat{y}_{i+\tau} \rangle .$$

If $F(\hat{x}_i)$ and $F(\hat{y}_i)$ represent the Fourier transforms of $\hat{x}_i$ and $\hat{y}_i$, then their cross spectrum, which is the Fourier transform of $r_{xy}(\tau)$, is

$$F(\hat{x}_i)F^*(\hat{y}_i)=A_x(f)A_y(f)e^{i[\phi_x(f)-\phi_y(f)]}.$$

Here $A_{x,y}(f)$ and $\phi_{x,y}(f)$, respectively, are the Fourier coefficient amplitudes and phase angles of $F(\hat{x}_i)$ and $F(\hat{y}_i)$. As suggested by [21], adding the same random phase sequence $\varphi(f)$ to the phase angles of the Fourier transform of $\hat{x}$ and $\hat{y}$ will preserve both the autocorrelations of each time series and the cross correlation upon transform inversion. The surrogate data pairs x_i' and y_i' will therefore be

$$x_i'=F^{-1}\{A_x(f)e^{i[\phi_x(f)+\varphi(f)]}\}$$

and

$$y_i'=F^{-1}\{A_y(f)e^{i[\phi_y(f)+\varphi(f)]}\}.$$

For each pair of experimental data sets $\hat{x}_i$ and $\hat{y}_i$, at least 19 separate surrogate data pairs x_i' and y_i' are generated, to permit a one-tailed nonparametric test of significance capable of rejecting the null hypothesis that these data are linearly synchronized at the 0.05 level [26].

APPENDIX B: CORRELATION STATISTICS

Given a time series z_i, the degree of correlation in time is given by the autocorrelation. For a given time lag $k=0,1,2,\ldots$, and time series length N, the autocorrelation $r_z(k)$ was estimated from

$$r_z(k)=\frac{\sum_{i=1}^{N-k}(z_i-\overline{z})(z_{i+k}-\overline{z})}{\sum_{i=1}^{N-k}(z_i-\overline{z})^2}$$

where $\overline{z}$ is the mean of z_i. The variance of the estimated autocorrelations at lags q beyond which the autocorrelation function is not significantly different from zero is [31]

$$\mathrm{var}[r_z(q)] \cong \frac{1}{N}\left(1+2\sum_{k=1}^{q} r(k)^2\right),$$

and the square root of this function is taken as the standard deviation. When the estimated autocorrelation is less than twice this standard deviation, the result is not significantly different from the value generated by white noise. In practice, all time series were detrended prior to estimation of the autocorrelation, with zero order detrending for unit responses (all ones and zeros corresponding to whether the unit fired or not), and first order detrending for all other data to remove both the mean and any simple linear drift from the time series.

Given two time series y_i and z_i, the degree of linear correlation between the two is measured by the cross correlation. The cross correlation $r_{yz}(k)$ can be estimated from the cross covariance $c_{yz}(k)$,

$$c_{yz}(k) = \begin{cases} \dfrac{1}{N}\displaystyle\sum_{i=1}^{N-k} (y_i-\overline{y})(z_{i+k}-\overline{z}), & k=0,1,2,\ldots \\ \dfrac{1}{N}\displaystyle\sum_{i=1}^{N+k} (z_i-\overline{z})(y_{i-k}-\overline{y}), & k=-1,-2,\ldots, \end{cases}$$

where $\overline{y}$ and $\overline{z}$ are the means of the time series. The cross correlation $r_{yz}(k)$ is recovered by normalizing $c_{yz}(k)$

$$r_{yz}(k) = \frac{c_{yz}(k)}{\dfrac{1}{N}\sqrt{\displaystyle\sum_{i=1}^{N-k}(z_i-\overline{z})^2 \sum_{i=1}^{N-k}(y_i-\overline{y})^2}}.$$

The variance of the estimated cross correlation at lags $\pm q$ beyond which the cross correlation function is not significantly different from zero may be estimated, again after [31]

$$\mathrm{var}[r_{yz}(q)] \cong \frac{1}{N-k}\sum_{k=-q}^{q} r_{yy}(k) r_{zz}(k)$$

and the square root of this function is taken as the standard deviation. When the estimated cross correlation is less than twice this standard deviation, it is not significantly different from two independent white noise processes.

Artifacts from significant autocorrelation in individual time series can create spurious cross correlation. These artifacts can be eliminated by filtering the data to ''prewhiten'' it prior to cross correlation estimation [1]. We tested all positive results suggesting significant cross correlation with the algorithm of Ljung and Glad [32], applying the same linear filter to both time series prior to cross correlation. Results that appeared spurious were rejected.

APPENDIX C: CALCULATING THE LARGEST SUB-LYAPUNOV EXPONENT FROM A DRIVE-RESPONSE SYSTEM

In this section, we briefly describe an algorithm for computing the largest sub-Lyapunov exponent from a unidirectionally coupled drive-response system. As a generalization of the unidirectionally coupled Hénon system in Sec. III A, we represent a general drive-response system in discrete time by the following pair of maps $\mathbf{f}:\mathbb{R}^m \to \mathbb{R}^m$ and $\mathbf{g}:\mathbb{R}^{n+m} \to \mathbb{R}^n$,

$$\begin{aligned} \mathbf{x}_{i+1} &= \mathbf{f}(\mathbf{x}_i), \\ \mathbf{y}_{i+1} &= \mathbf{g}(\mathbf{y}_i, \mathbf{x}_i, C), \end{aligned} \tag{C1}$$

where $\mathbf{x}$ is an m dimensional state vector in the driving system, $\mathbf{y}$ is an n dimensional state vector in the response system, and C is a scalar parameter in the response system $\mathbf{g}$ describing the strength of the coupling. Notice that the coupling (information flow) is one directional from the drive to the response, i.e., the m dimensional map $\mathbf{f}(\mathbf{x})$ is a function of the driver's state vector $\mathbf{x}$ only.

The asymptotic stability of the response system is determined by its largest sub-Lyapunov exponent λ. The largest sub-Lyapunov exponent gives the average exponential rate of divergence of two infinitesimally close by points, $(\mathbf{x}_0, \mathbf{y}_0)$ and $(\mathbf{x}_0, \mathbf{y}_0 + \mathbf{dy})$ in the response system. If we denote the initial deviation of two nearby points by

$$\mathbf{e}_0 = (\mathbf{x}_0, \mathbf{y}_0 + \mathbf{dy}) - (\mathbf{x}_0, \mathbf{y}_0),$$

then the magnitude of their deviation after t time steps in the future can be approximated by

$$|\mathbf{e}_t| \sim \exp(\lambda t)|\mathbf{e}_0|.$$

A negative λ signifies that any infinitesimally small errors between two different initial points in the response system will asymptotically converge to zero as t increases. Mathematically, λ is defined as the following limit:

$$\lambda = \lim_{t\to\infty} \frac{1}{t} \ln \frac{|\partial_{\mathbf{y}} \mathbf{g}^t(\mathbf{y}_0, \mathbf{x}_0, C)\hat{\mathbf{e}}_0|}{|\hat{\mathbf{e}}_0|}, \tag{C2}$$

where $\hat{\mathbf{e}}_0$ is the projection of $\mathbf{e}_0$ onto the n dimensional subspace of the response system, $\partial_{\mathbf{y}}\mathbf{g}^t$ is an $n \times n$ dimensional Jacobian matrix representing the derivatives of $\mathbf{g}^t$ with respect to the variable $\mathbf{y}$ only, and $\mathbf{g}^t$ is the tth iterated map of $\mathbf{g}$ (see Refs. [33,34] for more detailed descriptions of Lyapunov exponents). Here λ is assumed to be evaluated along a typical trajectory $(\mathbf{x}_0, \mathbf{y}_0), \ldots, \{(\mathbf{x}_t, \mathbf{y}_t) = (\mathbf{f}^t(\mathbf{x}_0), \mathbf{g}^t(\mathbf{y}_0, \mathbf{x}_0, C))\}$ of the drive-response system, Eqs. (1).

Using the chain rule, the Jacobian matrix of the tth iterated map, $\partial_{\mathbf{y}}\mathbf{g}^t(\mathbf{y}_0, \mathbf{x}_0, C)$, in Eq. (C2) can be rewritten as a product of t terms,

$$\begin{aligned} \partial_{\mathbf{y}}\mathbf{g}^t(\mathbf{y}_0, \mathbf{x}_0, C) = {} & \partial_{\mathbf{y}}\mathbf{g}(\mathbf{y}_{t-1}, \mathbf{x}_{t-1}, C) \cdots \partial_{\mathbf{y}}\mathbf{g}(\mathbf{y}_1, \mathbf{x}_1, C) \\ & \times \partial_{\mathbf{y}}\mathbf{g}(\mathbf{y}_0, \mathbf{x}_0, C), \end{aligned} \tag{C3}$$

where $\partial_{\mathbf{y}}\mathbf{g}(\mathbf{y}_i, \mathbf{x}_i, C)$, $0 \leq i \leq t-1$ is the Jacobian martrix of the map $\mathbf{g}$ with respect to $\mathbf{y}$ only, evaluated at the ith iterate of the orbit $(\mathbf{x}_i, \mathbf{y}_i)$.

The calculation of λ using Eqs. (C2) and (C3) can be numerically implemented in the following recursive procedure (see Ref. [35] for a detailed description of methods to compute all Lyapunov exponents of an arbitrary chaotic system).

To begin, we start with a random initial point $(\mathbf{x}_0,\mathbf{y}_0)$ on the attractor of the drive-response system and a random n dimensional unit vector $\hat{\mathbf{e}}_0$. Then we recursively define and calculate the following quantities for $i \geqslant 1$,

$$\alpha_i = |\partial_{\mathbf{y}}\mathbf{g}(\mathbf{y}_{i-1},\mathbf{x}_{i-1},C)\hat{\mathbf{e}}_{i-1}|, \quad \hat{\mathbf{e}}_i = \frac{\partial_{\mathbf{y}}\mathbf{g}(\mathbf{y}_{i-1},\mathbf{x}_{i-1},C)\hat{\mathbf{e}}_{i-1}}{\alpha_i}.$$

Here the scalar α_i is the magnitude of the vector $\partial_{\mathbf{y}}\mathbf{g}(\mathbf{y}_{i-1},\mathbf{x}_{i-1},C)\hat{\mathbf{e}}_{i-1}$, and serves to renormalize $\hat{\mathbf{e}}_i$ for each successive time step i. Using Eq. (C3), it is easy to see that

$$|\partial_{\mathbf{y}}\mathbf{g}^t(\mathbf{y}_0,\mathbf{x}_0,C)\hat{\mathbf{e}}_0| = \alpha_1 \ldots \alpha_t |\hat{\mathbf{e}}_t| = \alpha_1 \ldots \alpha_t,$$

and by Eq. (C2), λ can be approximated by the following finite time average:

$$\lambda \sim \frac{1}{t}\sum_{i=1}^{t} \ln\alpha_i .$$

[1] C. Chatfield, *The Analysis of Time Series*, 4th ed. (Chapman and Hall, London, 1989).

[2] L. M. Pecora, T. L. Carroll, and J. F. Heagy, in *Nonlinear Dynamics and Time Series: Building a Bridge Between the Natural and Statistical Sciences*, Fields Institute Communications Vol. 11, edited by C. D. Cutler and D. T. Kaplan (American Mathematical Society, Providence, RI, 1996).

[3] V. S. Afraimovich, N. N. Verichev, and M. I. Ravinovich, Izv. Vyssh. Uchebn. Zaved. Radiofiz. **29,** 1050 (1986) [Sov. Radiophys. Bol. **29**, 795 (1986)].

[4] N. F. Rulkov, M. M. Sushchik, L. S. Tsimring, and H. D. I. Abarbanel, Phys. Rev. E **51**, 980 (1995).

[5] F. Takens, Lecture Notes Math. **898**, 366 (1981): T. Sauer, J. Yorke, and M. Casdagli. J. Stat. Phys. **65,** 579 (1991).

[6] L. M. Pecora, T. L. Carroll, and J. F. Heagy, Phys. Rev. E **52**, 3420 (1995).

[7] L. Kocarev and U. Parlitz, Phys. Rev. Lett. **76**, 1816 (1996).

[8] L. M. Pecora and T. L. Carroll, Phys. Rev. Lett. **64,** 821 (1990).

[9] J. G. R. Jefferys, R. Traub, and M. A. Whittington, Trends Neurosci. **19**, 202 (1996).

[10] S. L. Bressler, R. Coppola, and R. Nakamura, Nature **366**, 153 (1993).

[11] H. C. Tuckwell, *Introduction to Theoretical Neurobiology: Volume 2 Nonlinear and Stochastic Theories* (Cambridge, Cambridge, 1988).

[12] J. J. Hopfield, Proc. Natl. Acad. Sci. U.S.A. **81**, 3088 (1982).

[13] W. R. Adey, Intern. J. Neurosci. **3**, 271 (1972).

[14] T. Chang, S. J. Schiff, T. Sauer, J.-P. Gossard, and R. E. Burke, Biophys. J. **67**, 671 (1994).

[15] S. J. Schiff, K. Jerger, T. Chang, T. Sauer, and P. G. Aitken, Biophys. J. **67**, 684 (1994).

[16] S. J. Schiff, K. Jerger, D. H. Duong, T. Chang, M. L. Spano, and W. L. Ditto, Nature **370**, 615 (1994).

[17] C. S. Sherrington, *The Integrative Action of the Nervous System* (Scribners, New York, 1909).

[18] V. Mountcastle, *Medical Physiology* (Mosby, St. Louis, MO, 1980).

[19] W. Rall and C. C. Hunt. J. Gen. Physiol. **39**, 397 (1956).

[20] J.-P. Gossard, M. K. Floeter, T. Chang, S. J. Schiff, and R. E. Burke, J. Neurophysiol. **72,** 1227 (1994).

[21] D. Prichard and J. Theiler, Phys. Rev. Lett. **73,** 951 (1994).

[22] A. M. Albano, J. Muench, C. Schwartz, A. I. Mees, and P. E. Rapp, Phys. Rev. A **38**, 3017 (1988).

[23] T. Sauer, in *Time Series Prediction: Forecasting the Future and Understanding the Past*, edited by A. S. Weigend and N. A. Gershenfeld, SFI Studies in the Sciences of Complexity, Proceedings Vol. XV (Addison-Wesley, Reading, MA, 1993), p. 175.

[24] T. Chang, T. Sauer, and S. J. Schiff, Chaos **5,** 118 (1995).

[25] S. J. Schiff, T. Sauer, and T. Chang, Integrative Physiol. Behavioral Sci. **29,** 246 (1994).

[26] A. C. A. Hope, J. R. Stat. Soc. B **30,** 582 (1968).

[27] D. T. Frazier, T. Narahashi, and M. Yamada, J. Pharm. Theor. **171,** 45 (1970).

[28] W. Rall, J. Cell Comput. Physiol. **46**, 413 (1955).

[29] B. J. Gluckman, T. I. Netoff, E. J. Neel, W. L. Ditto, M. L. Spano, and S. J. Schiff, Phys. Rev. Lett. (to be published).

[30] J. J. Collins, C. C. Chow, and T. T. Imhoff, Nature **376**, 236 (1995).

[31] G. E. P. Box and G. M. Jenkins, *Time Series Analysis, Forecasting and Control* (Holden-Day, Oakland, CA, 1976).

[32] L. Ljung and T. Glad, *Modeling of Dynamic Systems* (Prentice Hall, Englewood Cliffs, NJ, 1994).

[33] E. Ott, *Chaos in Dynamical Systems* (Cambridge University Press, Cambridge, 1993).

[34] S. H. Strogatz, *Nonlinear Dynamics and Chaos* (Addison-Wesley, Reading, MA, 1994)

[35] G. Benettin, L. Galgani, A. Giorgilli, and J.-M. Strelcyn, Meccanica **15**, 21 (1980).